Journal of Catalysis 274 (2010) 111–116

Contents lists available at ScienceDirect

Journal of Catalysis

journal homepage: www.elsevier.com/locate/jcat

On the nature and reactivity of active oxygen species formed from O_2 and N_2O on VO_x/MCM-41 used for oxidative dehydrogenation of propane

E.V. Kondratenko, A. Brückner *

Leibniz-Institut für Katalyse an der Universität Rostock e. V., Albert-Einstein-Straße 29a, D-18059 Rostock, Germany

ARTICLE INFO

Article history:
Received 19 April 2010
Revised 18 June 2010
Accepted 20 June 2010
Available online 23 July 2010

Keywords:
VO_x/MCM-41
Oxidative propane dehydrogenation
Oxygen radical anions
EPR
N_2O
Active species

ABSTRACT

Electron paramagnetic resonance (EPR) spectroscopy under controlled atmosphere conditions has been applied to elucidate the nature and reactivity of oxygen species formed upon reoxidation of a reduced VO_x(2.7 wt.%)/MCM-41 catalyst by gas-phase O_2 or N_2O. An electrophilic $V^{n+}\cdots O^{\cdot -}$ ($n = 4, 5$) radical anion intermediate is formed from O_2 probably via dissociation of a bi-atomic adsorbed oxygen species. This radical is remarkably stable in inert atmosphere up to elevated temperatures but reacts partly with C_3H_8 and almost completely with C_3H_6 and CO already at room temperature. In contrast, no such species could be observed upon reoxidation of reduced VO_x species with N_2O. This might be due to the rapid formation of nucleophilic O^{2-} oxide ions, which are not EPR-active. The different electronic nature of these oxygen intermediates is discussed as a reason for the higher propene selectivity obtained in propane oxidative dehydrogenation over VO_x/MCM-41 with N_2O.

1. Introduction

Oxidative dehydrogenation of light alkanes (e.g. propane) to the corresponding olefins (e.g. propene) is a true challenge for catalysis research since it opens attractive ways for converting cheap and abundant raw materials to valuable building blocks for the modern petrochemical industry. However, due to low olefin yields, such reactions are still far from their industrial applications. The major drawback is low olefin selectivity, which originates from fast consecutive oxidation of the target olefins to carbon oxides. Extensive research has been done in the past to improve the catalyst selectivity, and the relevant results have been reviewed during last 10 years [1–4]. Among the multitude of catalytic materials tested for the oxidative dehydrogenation of propane (ODP) to propene, high surface area (up to 1000 m^2/g) mesoporous silica materials possessing highly dispersed surface VO_x species belong to the best performing ones [5–15]. Maximum propene yields up to 25% have been obtained with these materials.

It has been repeatedly reported that the interaction between the oxide support and the deposited vanadium oxide determines the structure of VO_x species and their catalytic performance. Mesoporous silica materials provide high surface areas and, hence, the potential for high dispersion of the catalytically active surface VO_x sites. As a result, propene selectivity increases while the opposite effect was observed when V_xO_y surface clusters are present at high vanadium loadings and/or supports with lower surface area [6,10,13]. Furthermore, vanadium sites in tetrahedral oxygen coordination, being the major species on VO_x/MCM catalysts with low vanadium loadings, appeared to be less active but more selective than those in octahedral oxygen coordination [10]. Another advantage of mesoporous MCM-41 is the rather large pores and low intrinsic activity of highly dispersed VO_x species for the ODP reaction. As a result, mass transport within the pores does not limit the target reaction ensuring rapid diffusion of propene out of the pore system and, thus, reducing consecutive propene combustion. Besides the structure of VO_x species, surface acid–base properties determine the catalytic performance insofar as strongly acidic supports lower propene selectivities [16], while basic ones can improve it [17,18]. When using nitrous oxide instead of molecular oxygen as oxidizing agent, propene selectivity was also significantly improved over steam-activated iron-containing zeolites [19], bulk vanadium oxides [20] and supported vanadium-containing materials [13,21–23]. A similar effect of N_2O was also reported for the oxidative dehydrogenation of *n*-butane over vanadium–magnesium oxide catalysts [24]. Based on a kinetic analysis of the ODP reaction [13,14,25], the positive effect of N_2O on the ODP reaction was explained as follows. In contrast to O_2, reoxidation of reduced VO_x species is slower with N_2O, resulting in a lower steady-state concentration of active lattice oxygen sites. As a consequence, consecutive oxidation of propene to carbon oxides is

* Corresponding author. Fax: +49 381 1281 51244.
E-mail address: angelika.brueckner@catalysis.de (A. Brückner).

0021-9517/$ - see front matter © 2010 Elsevier Inc. All rights reserved.
doi:10.1016/j.jcat.2010.06.010

suppressed. In these studies, it has also been found that the activity of VO_x sites for consecutive propene oxidation increases with rising agglomerization degree [14]. However, propene selectivities did not differ much as long as the vanadium surface concentration remained below monolayer coverage, i. e., only isolated VO_x sites and small two-dimensional V_xO_y clusters but no V_2O_5 nanocrystallites were present. When the latter species were dominating, not only a dramatic drop of propene selectivity but also direct total oxidation of propane occurred with both oxidants, O_2 and N_2O, although this detrimental effect was less pronounced in presence of N_2O [14].

In addition to the above kinetic reasons, a recent steady-state isotopic transient kinetic analysis (SSITKA) study [26] suggested that compared to N_2O, other oxygen species (non-lattice oxygen of VO_x species) are formed from gas-phase O_2 and participate in CO_x formation. However, only limited experimental information is available on the nature of active oxygen species, which are formed from O_2 and N_2O upon reoxidation of reduced VO_x species. In early electron paramagnetic resonance (EPR) studies, the formation of O_2^-, $O^{\cdot-}$ and O_3^- anion radicals was postulated upon reaction of gas-phase O_2 with partially reduced V_2O_5/SiO_2 catalysts [27–29]. The corresponding EPR spectra are characterized by superhyperfine structure multiplets. This superhyperfine features were interpreted as arising from the interaction of the unpaired electron located on the oxygen anion radicals with the nuclear spin of the $^{51}V^{5+}$ cation, to which they were attached [27–29]. These oxygen species showed both high thermal stability up to 473 K and reactivity for oxidation of H_2, CH_4 and CO already at room temperature [29]. Based on this early work, similar EPR signals observed after oxygen adsorption on prereduced V silicalite [30] and after treatment of VS-1 with aqueous H_2O_2 [31] were assigned to $V(O_2^-)$ species. It was found that these species disappeared upon reaction with allyl alcohol or *n*-hexane. In a recent DFT study, the reoxidation of reduced V^{3+} and V^{4+} sites with O_2 and N_2O was evaluated [32]. These calculations suggest that a peroxovanadate species is formed when O_2 is adsorbed on a V^{3+} site. The formed peroxovanadate can decompose to yield a VO^{3+} vanadyl species and gas-phase O_2 or react with another reduced V^{3+} site to produce two vanadyl species. In contrast, when N_2O reacts with V^{3+}, a vanadyl species is restored and N_2 is formed. For analyzing the reaction of N_2O and O_2 with tetravalent vanadium, a $\equiv$V—OH species was assumed as initial state, from which hydrogen abstraction by N_2O or O_2 should lead to a VO^{3+} vanadyl site and $HO^{\cdot}$ or $HOO^{\cdot}$ radicals, respectively, as primary intermediates [32]. In this DFT study, the formation of vanadium sites coordinated by more than four oxygen ligands as well as vanadyl species with tetravalent vanadium, which in fact have been experimentally detected in VO_x/MCM catalysts [10,33,34], were not taken into account.

Based on the above background, it is the aim of this study to obtain experimental evidence on the nature and structure of oxygen species formed upon reoxidation of reduced highly dispersed VO_x species supported over MCM-41 with O_2 and N_2O. The same VO_x/MCM-41 catalyst used in this work has previously been thoroughly characterized and tested in the oxidative dehydrogenation of propane [13,14]. A turnover frequency of propane conversion of 0.016 mol_{C3H8} mol_V^{-1} s^{-1} has been measured with O_2 used as oxidizing agent. In comparison, the respective value with N_2O was only half as high, while the propene selectivity was higher, amounting to 80% with N_2O but only to 50% with O_2 at propane conversion of approximately 10%. Since several of the previously postulated oxygen species were paramagnetic, we applied EPR spectroscopy under controlled atmosphere conditions in order to experimentally identify oxygen species formed from gaseous N_2O and O_2 over VO_x/MCM-41 and to explore the reactivity of these species towards oxidation of C_3H_8, C_3H_6, and CO.

2. Experimental

2.1. Catalyst

The preparation and characterization of the supported VO_x/MCM-41 catalyst with a vanadium content of 2.7% has been described in detail in Ref. [13]. Briefly, the sample was prepared by impregnating an MCM-41 support synthesized according to literature procedures with the appropriate amount of vanadyl acetyl acetonate dissolved in toluene, followed by 12 h drying at 400 K and subsequent calcination for 12 h at 823 K. The vanadium loading was determined by ICP-OES after the calcination. The BET surface area and the average pore diameter of this material amount to 871 m^2/g and 2.78 nm, respectively. The formation of the mesoporous structure was confirmed by TEM analysis. UV-vis-DR and Raman spectra confirmed the prevalence of single VO_x surface sites besides some small VO_x clusters with V—O—V bonds, while the presence of nanocrystalline V_2O_5 has been safely excluded. From the BET surface area and the vanadium loading, an apparent surface density of 0.37 V/nm^2 has been estimated.

2.2. EPR measurements under controlled atmosphere conditions

EPR measurements were performed at 77 K on a Bruker ELEXSYS 500-10/12 cw-EPR spectrometer in X-band (microwave frequency $\approx$ 9.5 GHz) using an ER 4102ST rectangular cavity, and in Q-band (microwave frequency $\approx$ 35 GHz) using an ER 5106QT low temperature cylindrical cavity. A modulation amplitude of 100 kHz and a microwave power of 6.3 mW was applied. The magnetic field was measured with respect to the standard 2,2-diphenyl-1-picrylhydrazyl hydrate (DPPH).

Computer simulation of EPR spectra was performed with the program SIM14S of Lozos et al. [35] using the spin Hamiltonian

$$H = \mu_B \cdot S \cdot g \cdot B_0 + SAI \quad (1)$$

in which μ_B is the Bohr magneton, S is the electron spin operator, g is the g tensor, B_0 is the magnetic field vector, A is the hyperfine tensor and I is the nuclear spin operator.

17 mg of catalyst were filled into an EPR sample tube equipped with fittings for connection to a vacuum/gas dosing line. Prior to adsorption of O_2 or N_2O, the catalyst was treated in vacuum (10^{-5} mbar) at 773 K for 30 min. During this treatment, the sample color turned to dark gray due to reduction of V^{5+}.

3. Results

3.1. Nature of oxygen species formed upon adsorption of O_2 or N_2O on reduced VO_x/MCM-41

The EPR spectrum of as-prepared VO_x/MCM-41 is characterized by a hyperfine structure (hfs) signal, which is typical for axially distorted isolated V^{4+} species in octahedral or square-pyramidal coordination (spectrum 1 in Fig. 1B). However, a broad underlying singlet is also seen in this spectrum. This signal arises from magnetically interacting V^{4+} sites, suggesting that these species are connected with each other via an oxygen bridge, i.e. the VO_x/MCM-41 catalyst does not possess exclusively isolated vanadium sites. It should be stressed that the concentration of V^{4+} sites in the as-prepared catalyst was significantly lower than that of V^{5+}. The latter species were reduced during high-temperature (773 K) catalyst treatment in vacuum (10^{-5} mbar) as indicated by the change of the sample color from white to gray. However, the EPR signal belonging to V^{4+} species in octahedral or square-pyramidal coordination disappeared almost completely (spectrum 2 in Fig. 1B). Two reasons may be responsible for this effect: (1) change

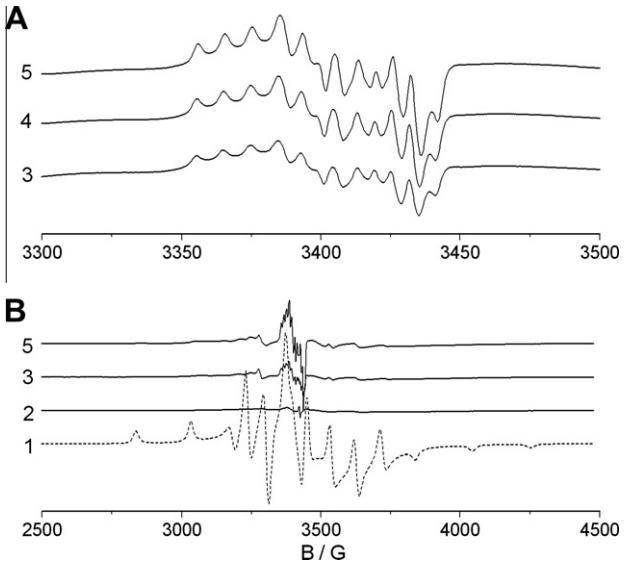

Fig. 1. EPR spectra measured at 77 K of as-prepared VO_x/MCM before any treatment (1), after 30-min evacuation at 773 K (2), after adsorption of 5 mbar O_2 at 77 K (3), after warming to room temperature for 1 min (4) and after storage for 1 h at room temperature (5). Plot B shows the overall spectra, while plot A shows the middle field range in more detail.

to tetrahedral coordination of V^{4+} due to the removal of adsorbed water and (2) deeper reduction to V^{3+}. Both of these species are not EPR-active at 77 K, due to short relaxation times [10,36]. Moreover, the zero-field splitting of V^{3+} with a total electron spin of $S = 1$ may be too large for an allowed spin transition to occur. The fact that there is still a small rest of the V^{4+} signal seen after evacuation at 773 K is an additional hint for the presence of some oligomerized V_xO_y clusters, in which vanadium species are usually octahedrally coordinated.

In order to prove if reduced VO_x species on MCM-41 can be oxidized, gas-phase O_2 (5 mbar) has been added to the reduced catalyst at 77 K. A multiline spectrum occurred in the middle field range (spectrum 3 in Fig. 1). This signal must be assigned to an oxygen radical directly bound to a V^{5+} atom since the line splitting comes from the superhyperfine structure (shfs) coupling of the electron spin at the oxygen radical with the nuclear spin of $^{51}V^{5+}$ ($S = 7/2$). This signal becomes more pronounced after a short warming to 293 K (spectrum 4 in Fig. 1A), indicating that more reduced vanadium sites have been oxidized. The oxygen radical does not decay after 1 h storage in O_2 at 293 K (spectrum 5 in Fig. 1A). Along with the oxygen signal, the hfs signal of octahedral V^{4+} species partly reappeared after reoxidation of reduced VO_x/MCM-41 (spectra 3 and 5 in Fig. 1B). Their formation can only be explained by electron transfer from V^{3+} (not visible by EPR under the actual measurement conditions) to oxygen, whereby octahedral V^{4+} is re-created.

For precise assignment of the shfs signal after oxygen adsorption in Fig. 1, the X-band spectrum has been reproduced by calculation using Eq. (1) (Table 1, Fig. 2). Excellent agreement between the experimental and calculated sum spectrum could be obtained

Table 1
Spin Hamiltonian parameters of the calculated spectrum 4 in Fig. 1A: I_{rel} – relative intensity; $g_{||}$, $g_\perp$ – parallel and perpendicular components of the g tensor; $A_{||}$, $A_\perp$ – parallel and perpendicular components of the hfs tensor; $\Delta B_{||}$, $\Delta B_\perp$ – width of the lines belonging to the parallel and perpendicular tensor components.

component	I_{rel}	$\Delta B_{||}/G$	$\Delta B_\perp/G$	$g_{||}$	$g_\perp$	$A_{||}/G$	$A_\perp/G$
1	1	2.29	6.55	2.0072	2.0236	6.69	9.77
2	1.6	5.04	32.76	1.9975	2.0244	–	–

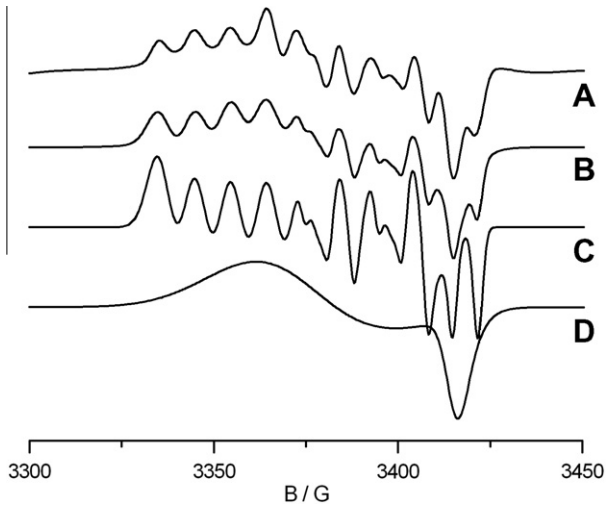

Fig. 2. (A) Experimental spectrum after adsorption of 5 mbar O_2 on reduced VO_x/MCM (compare Fig. 1A, spectrum 4), (B) sum spectrum calculated with the parameters in Table 1, (C and D) calculated spectra of components 1 and 2.

by superimposing two axial subsignals (Fig. 2) with the spin Hamiltonian parameters listed in Table 1.

To further clarify the specific nature of the formed oxygen radical, the EPR spectrum after adsorption of 5 mbar O_2 at 77 K on the prereduced VO_x/MCM-41 and short warming to 293 K has also been measured in Q-band at 148 K. Compared to the X-band measurements, higher microwave frequency and magnetic field in the Q-band setup provide a better resolution of the g tensor components. The corresponding spectrum is presented in Fig. 3. The g and A tensor components are most precisely obtained from the second derivative, in which the position of the shfs lines is reflected by minima and the broad background signal is suppressed. Since only two groups of eight shfs lines are observed, it can be concluded without any doubt that the oxygen radical species has axial symmetry. Moreover, the group of shfs signals at lower field shows approximately twice the intensity as the group at higher field, indicating that $g_\perp > g_{||}$ (Fig. 3). This is the typical situation for $O^{\cdot-}$ anion radicals [36–38]. Therefore, this shfs signal is assigned to a $V^{n+}\cdots O^{\cdot-}$ species ($n = 4$ or 5). This assignment will be further explained in Section 4.

In order to investigate the nature of oxygen species formed over reduced VO_x species from N_2O, we repeated the above EPR experiments with N_2O. After adsorption of 6 mbar N_2O at room temperature, the hfs signal of V^{4+} increases, which clearly indicates that V^{3+} formed during pretreatment in vacuum must have been oxi-

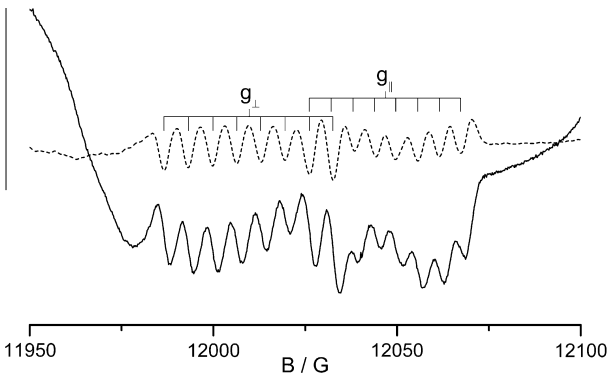

Fig. 3. EPR spectrum after adsorption of 5 mbar O_2 measured in Q-band at 148 K: solid line – 1st derivative, dashed line – 2nd derivative.

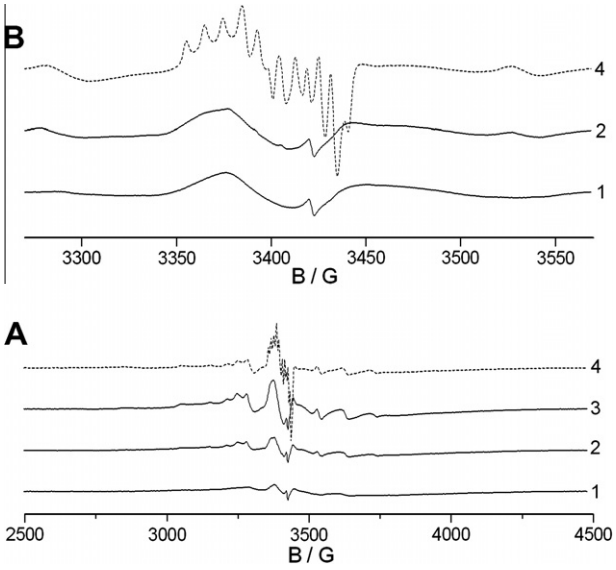

Fig. 4. EPR spectra measured at 77 K after the following sequence of treatment: (1) 1 h evacuation (10^{-5} mbar) at 773 K, (2) adsorption of 6 mbar N_2O at 293 K, short evacuation at 293 K to remove residual gaseous N_2O, (3) adsorption of 6 mbar N_2O at 323 K, short evacuation at 293 K, and (4) adsorption of 6 mbar N_2O + 3 mbar O_2 at 293 K, short evacuation at 293 K. Plot A shows the overall spectra, while plot B shows the middle field range in more detail.

dized by N_2O. This process is even more pronounced when N_2O is adsorbed at 323 K (Fig. 4, spectra 1–3). Yet, in contrast to the respective experiment with O_2 (compare Fig. 1), no shfs signal of $V^{n+}\cdots O^{\cdot-}$ is observed. This, however, appears immediately, when 3 mbar of O_2 are supplied in addition to the 6 mbar N_2O (Fig. 4, spectrum 4). This experiment strongly suggests that different oxygen species are formed from O_2 and N_2O. N_2O reoxidises reduced VO_x species yielding diamagnetic O^{2-} species (lattice oxygen of vanadia). This experimental result is in agreement with previous DFT calculations [32].

3.2. Reactivity of adsorbed oxygen species against propane, propene and carbon monoxide

The reactivity of oxygen species formed upon reoxidation of reduced VO_x species by O_2 was investigated by in-situ EPR in the following way. After these oxygen species were formed as described in Section 3.1, propane was fed to the EPR sample tube at different temperatures for various times followed by quenching to 77 K. Hereafter, EPR spectra were recorded at 77 K. In order to be sure that the oxygen species reacted with C_3H_8 but did not thermally disappear, the same procedure was performed in parallel with a second sample using N_2 (inert gas) instead of C_3H_8. Fig. 5 compares the EPR spectra recorded during these two tests. It can be seen that the intensity of the shfs signal decreases strongly already after 5 min contact with C_3H_8 at 293 K. This signal practically disappears after further contact with C_3H_8 for 30 min at 293 K and for 5 min at 303 K. When N_2 was used instead of C_3H_8, the shfs signal was still widely unchanged. This proves that C_3H_8 can react with $V^{n+}\cdots O^{\cdot-}$ already at room temperature, while thermal decline in inert gas requires much more severe conditions.

When C_3H_6 was used as reactant, the $V^{n+}\cdots O^{\cdot-}$ shfs signal is already gone at 293 K, leaving behind only the hyperfine structure (hfs) signal arising from the coupling of the unpaired electron at the V^{4+} with the nuclear spin of ^{51}V (black line in Fig. 6). This shows clearly that C_3H_6 is much more reactive than C_3H_8, since it consumes the $O^{\cdot-}$ species completely already at room temperature. Interestingly, there is also a slight shift of the position of the hfs

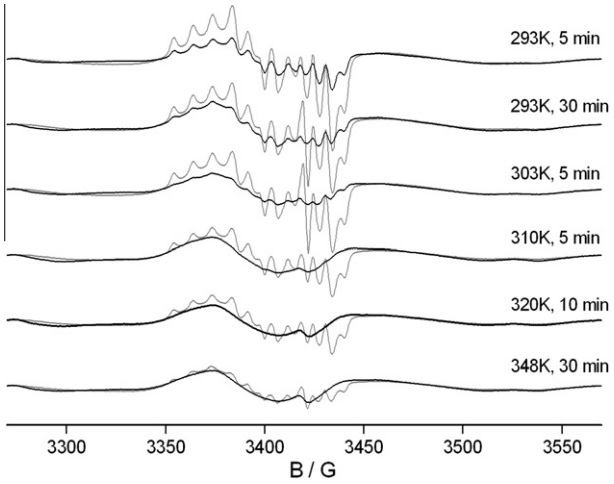

Fig. 5. EPR spectra measured at 77 K after the following treatment: 1 h evacuation (10^{-5} mbar) at 773 K, adsorption of 5 mbar O_2 at 293 K, short evacuation at 293 K to remove residual gaseous O_2, filling the sample tube with 1 bar N_2 (gray lines) or 1 bar propane (black lines) and heating for different times at different temperatures as indicated.

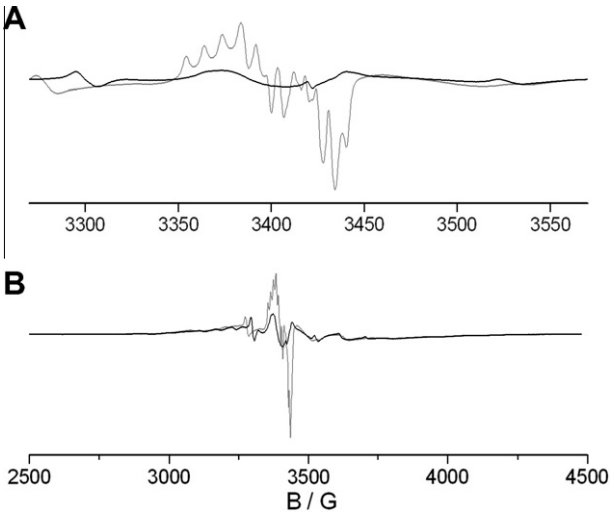

Fig. 6. EPR spectra measured at 77 K after the following treatment: 1-h evacuation (10^{-5} mbar) at 773 K, adsorption of 5 mbar O_2 at 293 K, short evacuation at 293 K to remove residual gaseous O_2, filling the sample tube with 1 bar N_2 (gray lines) or 1 bar propene (black lines) at 293 K. Plot B shows the overall spectra while plot A shows the middle field range in more detail.

lines upon reaction with C_3H_6 (Fig. 6B), suggesting that the local coordination geometry of the V^{4+} site is changed upon removal of $O^{\cdot-}$.

Besides C_3H_8 and C_3H_6, the interaction of the $V^{n+}\cdots O^{\cdot-}$ site with CO was also studied (Fig. 7). It turns out that CO shows a similar reactivity like C_3H_6. Only traces of the shfs signal remain after 5 min contact at 293 K with a mixture of 5% CO in He at 1 bar. This signal completely disappeared after 30 min at 293 K.

4. Discussion

X-band shfs signals with similar multiline features like those in Fig. 1 have been previously reported by Kazansky et al. after oxygen adsorption on a partially reduced V_2O_5/SiO_2 catalyst [27]. These signals have been phenomenologically attributed to a rhombic $V^{5+}\cdots O_2^{\cdot-}$ species, formed upon electron transfer from V^{4+} to

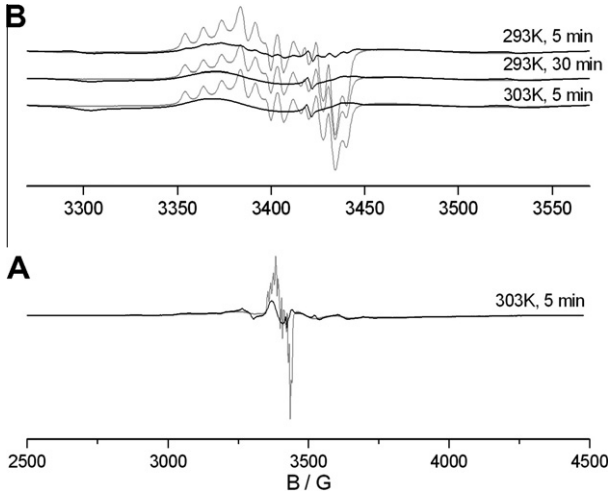

Fig. 7. EPR spectra measured at 77 K after the following treatment: 1 h evacuation (10^{-5} mbar) at 773 K, adsorption of 5 mbar O_2 at 293 K, short evacuation at 293 K to remove residual gaseous O_2, filling the sample tube with 1 bar N_2 (gray lines) or 1 bar of a 5% CO/He mixture (black lines) at 293 K and keeping under the indicated conditions. Plot B shows the overall spectrum after 5 min storage at 303 K, while plot A shows the middle field range of all spectra in more detail.

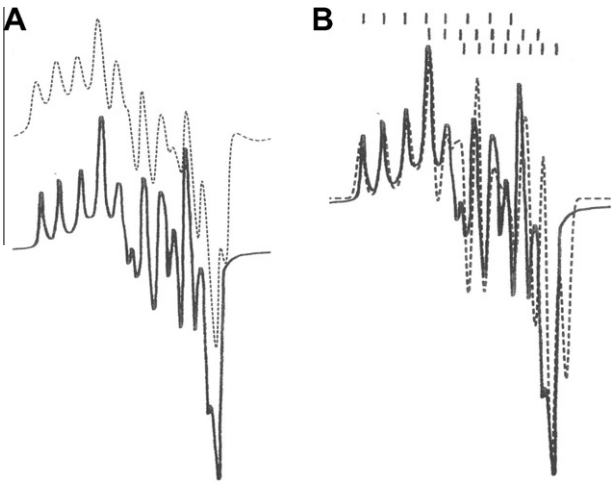

Fig. 8. Experimental EPR spectrum published by Kazansky et al. [25] (solid line) in comparison with (A) spectrum 3 from Fig. 1 of this work (dashed line) and (B) the spectrum calculated with the spin Hamiltonian parameters published by Kazansky et al. [25] (dashed line).

O_2. For comparison, the spectrum published in this previous paper is plotted in Fig. 8A together with the spectrum recorded in the present study after adsorption of 5 mbar of O_2 at 77 K (spectrum 3 in Fig. 1A). Similarities of both signals are obvious. The following spin Hamiltonian parameters were derived by Kazansky et al. [27] from their EPR spectrum just by simple measuring: $g_1 = 2.023$, $g_2 = 2.011$, $g_3 = 2.004$, $A_1 = 9.7$ G, $A_2 = 6.8$ G, $A_3 = 5.9$ G. However, when we tried to reproduce their experimental spectrum by simulation using these reported spin Hamiltonian parameters, no satisfactory agreement was obtained (Fig. 8B). Thus, the assignment of this EPR signal to a rhombic $V^{5+}\cdots O_2^{\cdot-}$ species appears to be highly doubtful. We were not able either to fit our EPR spectrum in Fig. 1A using rhombic g and A tensors, as appropriate for an $O_2^{\cdot-}$ species. However, as mentioned in Section 3.1, an excellent fit could be obtained by superimposing two subspectra with axial g tensor parameters, one with and the other without shfs (Table 1, Fig. 3). From this fit and in accordance with the experimental Q-band spectrum, it is evident that $g_\perp > g_{||}$. According to theory [38], the relation of the g values of an axial $O^{\cdot-}$ species is $g_\perp > g_{||}$ since $g_{||} = g_{zz} \approx g_e$ and $g_\perp = g_{xx} = g_{yy} = g_e + (2\lambda/\Delta E)$, λ being the spin-orbit coupling constant and ΔE being the energy difference between the p_z and the degenerate p_x and p_y orbitals of oxygen. This relation is obeyed for a wide variety of oxide systems accommodating $O^{\cdot-}$ species [38] and holds also for spectra 3–5 in Fig. 1A. Therefore, we assign the subline with shfs (component 1 in Table 1, Fig. 2C) to a $V^{5+}\cdots O^{\cdot-}$ species. Oxygen in this species is directly bound to V^{5+} but has one electron less than a lattice oxide ion. Moreover, there is no interaction between this oxygen and any paramagnetic species. In other words, this $V^{5+}\cdots O^{\cdot-}$ species should be an isolated species

For the broad subsignal of component 2, the condition $g_\perp > g_{||}$ is also fulfilled (Table 1, Fig. 2D). The shape of this subline is very similar to that of $O^{\cdot-}$ species without shfs, e. g. in Mo/SiO_2 catalysts [29]. Taking into account these previous data and the formation of V^{4+} after adsorption of O_2 over reduced VO_x/MCM-41 in our study (Fig. 1B, spectra 3 and 5), the broad subsignal can be ascribed to a $O_xV^{4+}\cdots O^{\cdot-}$ species. In contrast to the $O_xV^{5+}\cdots O^{\cdot-}$ species, the superhyperfine structure in the spectrum of $O_xV^{4+}\cdots O^{\cdot-}$ is averaged out due to the magnetic interaction between the electron spins of $O^{\cdot-}$ and V^{4+}. We suggest that the $O_xV^{4+}\cdots O^{\cdot-}$ species is part of a VO_x aggregate consisting of at least two vanadium atoms with $O^{\cdot-}$ being in the bridging position between two vanadium atoms. This agrees also with previous catalytic results, which suggest that single VO_x sites and small two-dimensional V_xO_y clusters show similar activity [14]. In summary, based on the present experimental and theoretical results, we ascribe the EPR signals with shfs and without shfs to $O_xV^{5+}\cdots O^{\cdot-}$ and $O_xV^{4+}\cdots O^{\cdot-}$ species, respectively.

In the following, we discuss a mechanistic proposal for the formation of EPR-active and non-active species upon reoxidation of reduced VO_x/MCM-41 with O_2 and N_2O based on the present experiments and previous DFT results [32]. In agreement with the DFT study, our experimental analysis proves that the reoxidation of O_xV^{4+} and O_xV^{3+} by O_2 is straightforward, because this happens even at 77 K. Fig. 9A summarizes main pathways and reaction species upon reoxidation of O_xV^{4+} and O_xV^{3+} by O_2. $O_xV^{4+}\cdots O_2^{\cdot-}$ in this scheme should be paramagnetic and, thus, EPR-active. The reason that it was not observed in our study may be its very fast conversion into a peroxovanadate species, $O_xV^{5+}\cdots O_2^{2-}$, which is energetically favoured [32]. The DFT calculations have also shown that this peroxovanadate should not be stable above 800 K and decompose to $O{=}V^{5+}O_3$ and ½ O_2 or to two $O{=}V^{5+}O_3$, when a V^{3+} site is additionally involved. Likewise, the $O_xV^{5+}\cdots O^{\cdot-}$ species observed in the EPR spectra could be formed by reaction of

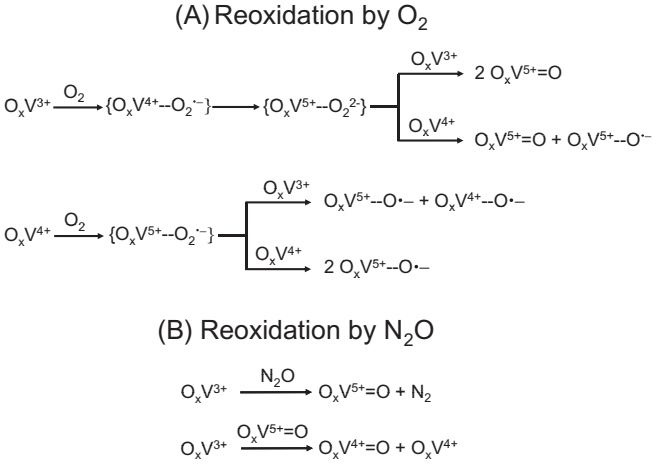

Fig. 9. Suggested pathways for reoxidation of O_xV^{3+} and O_xV^{4+} by O_2 and N_2O.

$O_3V^{5+}\cdots O_2^{2-}$ with a second O_xV^{4+} site. Obviously, this happens already at very low temperature. At elevated temperatures, the $O_xV^{5+}\cdots O^{\cdot-}$ moiety declines by forming a vanadyl species.

Upon reoxidation of O_xV^{4+}, a $O_xV^{5+}\cdots O_2^{\cdot-}$ species should initially be formed (Fig. 9A, bottom line). This species is suggested to be very short-lived because its EPR signal was not detected. It can react with another O_xV^{4+} or O_xV^{3+} species to yield $O_xV^{5+}\cdots O^{\cdot-}$ and $O_xV^{4+}\cdots O^{\cdot-}$. Both species are observed by EPR in our study (Fig. 2, spectra C and D).

When N_2O reacted with reduced VO_x species, no EPR-active oxygen radical species were detected. Obviously, a hypothetic $V^{n+}\cdots O^{\cdot-}$ intermediate, if formed at all, is too short-lived in this case. Possible reaction pathways are summarized in Fig. 9B. According to DFT results in [32], the reoxidation of O_xV^{4+} with N_2O requires a ca. 100 kJ/mol higher activation energy compared to that of $(O)_xV^{3+}$. Therefore, it was assumed that only O_xV^{3+} species can be reoxidized by N_2O in the temperature range from 77 to 300 K. Both O_xV^{5+}=O and O_xV^{4+} originating from O_xV^{3+} are EPR-silent, while O_xV^{4+}=O was experimentally observed.

The difference in the nature of surface oxygen species formed from O_2 and N_2O could also be the reason for the different catalytic performance observed in the ODH of propane over VO_x/MCM-41 with O_2 and N_2O [13,14]. The higher activity but lower propene selectivity with O_2 might be due to the formation of $O_xV^{5+}\cdots O_2^{\cdot-}$, $O_xV^{5+}\cdots O_2^{2-}$, and $V^{n+}\cdots O^{\cdot-}$. The latter species was experimentally proven to be very active, reacting with propane partially and with propene even completely already at room temperature. Since the primary step of interaction of gas-phase O_2 with a reduced VO_x site should not depend on temperature, it can be safely expected that such species are also formed under true ODH conditions and react even faster with the hydrocarbons. In addition, peroxovanadates are also highly reactive for consecutive propene oxidation to CO_x as theoretically predicted in [32]. In contrast, such highly reactive species are not formed with N_2O. In this case, the reaction probably proceeds by participation of nucleophilic oxide ions. This might also be the reason for the higher propene selectivity in the ODP reaction with N_2O.

Interestingly, the fact whether $O^{\cdot-}$ species are formed from O_2 or N_2O seems to depend very much on the nature of the catalyst. Thus, Panov et al. have shown that the highly active α-oxygen species in FeZSM-5, being able to oxidize benzene to phenol at room temperature with almost 100% selectivity, are $O^{\cdot-}$ species, too. However, in contrast to VO_x/SiO_2 catalysts, $O^{\cdot-}$ species in FeZSM-5 are exclusively formed upon reoxidation of prereduced Fe^{2+} sites by N_2O, but not by O_2 [39–42]. This surprising difference could be related to the different redox potential of the active metal ions and/or to the local pore environment, in which the latter are located. Further research is certainly needed to clarify this issue.

5. Conclusions

By EPR measurements under controlled atmosphere conditions at two different microwave frequencies (X- and Q-band), the formation of a $V^{n+}\cdots O^{\cdot-}$ ($n = 4, 5$) radical anion species has been detected on the surface of a prereduced 2.7 wt.% VO_x/MCM-41 catalyst after contact with gas-phase O_2 and identified by spectra simulation. The previously claimed formation of a molecular $V^{n+}\cdots O_2^{\cdot-}$ oxygen radical [27] could not be confirmed. The $V^{n+}\cdots O^{\cdot-}$ species was found to be surprisingly stable in inert N_2 atmosphere, being weakly visible even after 30 min at 348 K. However, it reacts to a considerable extent with C_3H_8 already at room temperature and is completely consumed by C_3H_6 and CO under the same conditions. In contrast, neither such paramagnetic $V^{n+}\cdots O^{\cdot-}$ site nor any other EPR-active oxygen radical species could be detected upon reoxidation of the same prereduced VO_x/MCM-41 by N_2O. Since it is well known that N_2O readily deposits its oxygen on the surface of partially reduced oxide by releasing N_2, it is probable that this happens on prereduced VO_x/MCM as well. From the fact that no $O^{\cdot-}$ is evidenced by EPR, we conclude that transfer of a second electron might be very fast and a diamagnetic O^{2-} oxide ion is formed and incorporated in the catalyst structure. The higher activity and lower selectivity observed in the ODH of propane with O_2 in comparison with N_2O is attributed to the presence of highly reactive electrophilic $O^{\cdot-}$ species in the former case (which preferentially burn propene), while nucleophilic, less active but more selective O^{2-} ions serve as reactants in ODH of propane with N_2O.

References

[1] H.H. Kung, Adv. Catal. 40 (1994) 1.
[2] E.A. Mamedov, V. Cortés Corberán, Appl. Catal. A 127 (1995) 1.
[3] M. Baerns, G. Grubert, E.V. Kondratenko, D. Linke, U. Rodemerk, Oil Gas Eur. Mag. 1 (2003) 36.
[4] R. Grabowski, Catal. Rev. Sci. Eng. 48 (2006) 199.
[5] J. Santamaria-González, J. Luque-Zambrana, J. Mérida-Robles, P. Maireles-Torres, E. Rodríguez-Castellón, A. Jiménez-López, Catal. Lett. 68 (2000) 67.
[6] O.V. Buyevskaya, A. Brückner, E.V. Kondratenko, D. Wolf, M. Baerns, Catal. Today 67 (2001) 369.
[7] J.M. López Nieto, Top. Catal. 15 (2001) 189.
[8] B. Solsona, T. Blasco, J.M. López Nieto, M.L. Pena, F. Rey, A. Vidal-Moya, J. Catal. 203 (2001) 443.
[9] Q. Zhang, Y. Wang, Y. Ohishi, T. Shishido, K. Takehira, J. Catal. 202 (2001) 308.
[10] A. Brückner, P. Rybarczyk, H. Kosslick, G.-U. Wolf, M. Baerns, Stud. Surf. Sci. Catal. 142 (2002) 1141.
[11] Y.-M. Liu, Y. Cao, N. Yi, W.-L. Feng, W.-L. Dai, S.-R. Yan, H.-Y. He, K.-N. Fan, J. Catal. 224 (2004) 417.
[12] Y.-M. Liu, W.-L. Feng, T.-C. Li, H.-Y. He, W.-L. Dai, W. Huang, Y. Cao, K.-N. Fan, J. Catal. 239 (2006) 125.
[13] E.V. Kondratenko, M. Cherian, M. Baerns, X. Su, R. Schlögl, X. Wang, I.E. Wachs, J. Catal. 234 (2005) 131.
[14] O. Ovsitser, M. Cherian, E.V. Kondratenko, J. Phys. Chem. C 111 (2007) 8594.
[15] S.A. Karakoulina, K.S. Triantafyllidis, A.A. Lemonidou, Micropor. Mesopor. Materials 110 (2008) 157.
[16] E.V. Kondratenko, N. Steinfeldt, M. Baerns, Phys. Chem. Chem. Phys. 8 (2006) 1624.
[17] C. Pak, A.T. Bell, T.D. Tilley, J. Catal. 206 (2002) 49.
[18] G. Garcia Cortez, J.L.G. Fierro, M.A. Banares, Catal. Today 78 (2003) 219.
[19] J. Pérez-Ramírez, A. Gallardo-Llamas, J. Catal. 223 (2004) 382.
[20] E.V. Kondratenko, O. Ovsitser, J. Radnik, M. Schneider, R. Kraehnert, U.U. Dingerdissen, Appl. Catal. A 319 (2007) 98.
[21] E.V. Kondratenko, M. Baerns, Appl. Catal. A 222 (2001) 133.
[22] E.V. Kondratenko, M. Cherian, M. Baerns, Catal. Today 99 (2005) 59.
[23] E.V. Kondratenko, M. Cherian, M. Baerns, Catal. Today 122 (2006) 60.
[24] J.M. López Nieto, A. Dejoz, M.I. Vazquez, W. O'Leary, J. Cunningham, Catal. Today 40 (1998) 215.
[25] O. Ovsitser, M. Cherian, A. Brückner, E.V. Kondratenko, J. Catal. 265 (2009) 8.
[26] O. Ovsitser, E.V. Kondratenko, Catal. Today 142 (2009) 138.
[27] V.A. Shvets, V.M. Vorontinzev, V.B. Kazansky, J. Catal. 15 (1969) 214.
[28] B.N. Shelimov, C. Naccache, M. Che, J. Catal. 37 (1975) 279.
[29] V.A. Shvets, V.B. Kazansky, J. Catal. 25 (1972) 123.
[30] G. Centi, S. Perathoner, F. Trifiro, A. Aboukais, C.F. Aissi, M. Guelton, J. Phys. Chem. 96 (1992) 2617.
[31] V.N. Shetti, M.J. Rani, D. Srinavas, P. Ratnasamy, J. Phys. Chem. B 110 (2006) 677.
[32] X. Rozanska, E.V. Kondratenko, J. Sauer, J. Catal. 256 (2008) 84.
[33] S. Sylesh, A.P. Singh, J. Catal. 233 (2005) 359.
[34] S. Zamani, V. Meynen, A.-M. Hanu, M. Mertens, E. Popovici, S. Van Doorslaer, P. Cool, Phys. Chem. Chem. Phys. 11 (2009) 5823.
[35] G.P. Lozos, B.M. Hofman, C.G. Franz, Quantum Chem. Prog. Exchange 265 (1973).
[36] J.C. Vedrine, in: F. Delanny, (Ed.), Characterization of Heterogeneous Catalysts, Marcel Dekker Inc., New York, 1984, p. 161.
[37] J.H. Lunsford, Adv. Catal. 22 (1972) 265.
[38] M. Che, A.J. Tench, Adv. Catal. 32 (1983) 1.
[39] G.I. Panov, K.A. Dubkov, E.V. Starokon, Catal. Today 117 (2006) 148.
[40] V.S. Chernyavsky, L.V. Pirutko, A.K. Uriate, A.S. Kharitonov, G.I. Panov, J. Catal. 245 (2007) 466.
[41] G.I. Panov, E.V. Starokon, L.V. Pirutko, E.A. Paukshtis, V.A. Parmon, J. Catal. 254 (2008) 110.
[42] L.V. Pirutko, V.S. Chernyavsky, E.V. Starokon, A.A. Ivanov, A.S. Kharitonov, G.I. Panov, Appl. Catal. B 91 (2009) 174.